https://doi.org/10.5194/os-2019-57
Preprint. Discussion started: 11 June 2019

Ocean Science
Discussions
Open Access
EGU

Photoproduction of nitric oxide in seawater

Ye Tian[1,2,3], Gui–Peng Yang[1,2,3], Chun–Ying Liu[1,2,3], Pei–Feng Li[3], Hong–Tao Chen[1,2,3], Hermann W. Bange[4]

[1]Key Laboratory of Marine Chemistry Theory and Technology, Ministry of Education, Qingdao, 266100, China
[2]Laboratory for Marine Ecology and Environmental Science, Qingdao National Laboratory for Marine Science and Technology, Qingdao 266071, China
[3]College of Chemistry and Chemical Engineering, Ocean University of China, Qingdao, 266100, China
[4] GEOMAR Helmholtz–Zentrum für Ozeanforschung Kiel, Kiel, 24105, Germany

Correspondence to: Chun–ying Liu (roseliu@ouc.edu.cn) and Hong–Tao Chen (chenht@ouc.edu.cn)

Abstract. Nitric oxide (NO) is a short–lived intermediate of the oceanic nitrogen cycle. However, our knowledge about its production and consumption pathways in oceanic environments is rudimentary. In order to decipher the major factors affecting NO photochemical production, we irradiated artificial seawater samples as well as natural surface seawater samples in laboratory experiments. The seawater samples were collected during a cruise to the western tropical North Pacific Ocean (WTNP) from November 2015 to January 2016. NO photoproduction rates from dissolved nitrite in artificial seawater showed increasing trends with decreasing pH, increasing temperatures and increasing salinity. In contrast, NO photoproduction in from the natural seawater samples from the WTNP did not show any correlations with pH, water temperature and salinity as well as dissolved nitrite concentrations. NO photoproduction rates in the WTNP were significantly larger than the NO air–sea flux densities indicating a further NO loss process in the surface layer.

1 Introduction

Nitric oxide (NO) is a short–lived intermediate of the oceanic nitrogen cycle, see e.g. Bange (2008) and Kuypers et al. (2018). There are only a few reports about oceanic NO so far because of its reactivity the determination is challenging (Liu et al., 2017; Lutterbeck and Bange, 2015;Zafiriou et al., 1980). NO is produced and consumed during various microbial processes such as nitrification, denitrification and anammox (Schreiber et al. 2012; Kuypers et al., 2018). Moreover, it is known that both phytoplankton and zooplankton can metabolize NO and are influenced by ambient (extracellular) NO concentrations (Astier et al., 2018; Singh and Lal, 2016; Wang et al., 2017).

https://doi.org/10.5194/os-2019-57
Preprint. Discussion started: 11 June 2019

Apart from (micro)biological processes, NO can be produced photochemically from dissolved nitrite (NO_2^-) in the sunlit surface ocean (Zafiriou and True, 1979; Zafiriou and McFarland, 1981):

$$NO_2^- + H_2O \xrightarrow{h\nu} NO + {\bullet}OH + OH^-, \quad (1)$$

Photochemical production of NO have been measured in the surface waters of the equatorial Pacific Ocean (Zafiriou et al., 1980; Zafiriou and McFarland, 1981), the Seto Inland Sea (Anifowose and Sakugawa, 2017; Olasehinde et al., 2009; 2010), the Bohai and Yellow Seas (Liu et al., 2017, Tian et al., 2018) and the Kurose River (Japan) (Olasehinde et al., 2009; Anifowose et al., 2015).

In this study, we present the results of our measurements of NO photoproduction in laboratory experiments using artificial and natural seawater samples. The major objectives of our studies were (i) to decipher the factors affecting NO photoproduction in seawater, (ii) to determine the photoproduction rates of NO from samples collected during a cruise to the western tropical North Pacific Ocean (WTNP) and (iii) to quantify the role of photoproduction as a source of NO in the surface waters of the WTNP.

2 Methods

2.1 Determination of dissolved NO in aqueous samples

For the measurements of dissolved NO we applied the method described by Olasehinde et al. (2009): In brief, NO in the aqueous samples was determined by trapping it with added 4,5–diaminofluorescein (DAF–2, chromatographic grade from Sigma–Aldrich, USA) and measuring the reaction product triazolofluorescein (DAF–2T) with a high performance liquid chromatography system (HPLC). We used an Agilent 1260 Infinity HPLC (Agilent Technologies Inc., USA) system equipped with a Venusil XBP–C18 column (5.0 µm; 4.6 mm × 250 mm i.d.). The column temperature was set to 25°C and the mobile phase was comprised of acetonitrile (HPLC grade from Merck, Darmstadt, Germany) and phosphate buffer (disodium hydrogen phosphate heptahydrate, guaranteed reagent from Sinopharm Chemical Reagent Co., Ltd, Shanghai, China) solution (10 mmol L^{-1} at pH 7.4) with a ratio of 8:92 (*v*:*v*) and a flow rate of 1 mL min^{-1} in the isocratic mode.

The injected sample volume was 5.0 µL. The eluate was analyzed with a fluorescence diode array detector at wavelengths of 495 and 515 nm for excitation and emission, respectively. The retention time of DAF–2T was about 5.5 min.

https://doi.org/10.5194/os-2019-57
Preprint. Discussion started: 11 June 2019

The detection limit of dissolved NO in Milli–Q water was 9.0×10^{-11} mol L^{-1} and average relative standard error of the NO measurements was +/– 5.7 % at a concentration of 3×10^{-9} mol L^{-1}.

2.2 Set–up of irradiation experiments

We performed irradiation experiments with Milli–Q water (18.2 MΩ cm, Millipore Company, USA), artificial seawater and natural seawater samples. Artificial seawater was prepared by dissolving 23.96 g NaCl, 5.08 g $MgCl_2$, 3.99 g Na_2SO_4, 1.12 g $CaCl_2$, 0.67 g KCl, 0.20 g $NaHCO_3$, 0.10 g KBr, 0.03 g H_3BO_3 and 0.03 g NaF in 1 L of Milli–Q water (Bajt et al., 1997) and filtered by 0.2 µm polyethersulfone membrane (Pall, USA) before the experiments.

All irradiation experiments (except the experiments for the temperature dependence, see section below) were conducted at a constant temperature of 20 ℃ by controlling the temperature of thermostat water bath (LAUDA Dr. R. Wobser Gmbh & Co. KG, Germany). The volume of the irradiated aqueous solution was 10 mL which was placed in a stoppered quartz glass tube. All quartz glass tubes were treated in the same manner except the tubes wrapped in aluminum foil which served as dark control.

Milli–Q water and artificial seawater samples were spiked with varying amounts of $NaNO_2$ (puriss. p.a. ACS grade from Sigma–Aldrich, USA; for details see sections below). All other chemicals were of analytical grade from Tianjin Kemiou Chemical Reagent Co., Ltd or Shanghai Sinopharm Chemical Reagent Co., Ltd.

Triplicate samples from each treatment were collected every 0.5 h with an entire irradiation time of 2 h. The data from the experiments with Milli–Q and artificial seawater samples were fitted with a simple linear regression in artificial seawater samples (see below). However, a linear relationship was not found > 30 min for the natural seawater samples and, therefore, we decided to choose 30 min as the total experimental time for seawater samples. Statistical analyses were done using SPSS v.16.0 or Origin 9.0 and results were considered significant at $p \leq 0.05$.

The artificial light source was a 1 kW xenon lamp, which provided a light intensity of 765 W m^{-2}. The illuminance was about 60,000 lx (measured with an instrument of Zhejiang Top Cloud–Agri Technology Co., Ltd, China). The lamp was installed in an immersion well photochemical reactor called SUNTEST CPS+ solar simulator produced by ATLAS, Germany. The solar simulator employed in this study has been demonstrated to produce spectra which mimics that of the solar radiation and emits a radiation of wavelength from 300 to 800 nm (Wu et al., 2015).

https://doi.org/10.5194/os-2019-57
Preprint. Discussion started: 11 June 2019

2.3 Experimental outline

2.3.1 Optimal DAF–2 concentration and storage time

In order to find out the optimal DAF–2 concentration, 10 mL of artificial seawater containing 0.5 μmol L^{-1} NO_2^- was irradiated with various concentrations of DAF–2 ranging from 0.7 μmol L^{-1} to 4.8 μmol L^{-1} for 2 h.

To ascertain the sample storage time, 10 mL with artificial seawater samples containing 5.0 μmol L^{-1} or 0.5 μmol L^{-1} NO_2^- were irradiated with various concentrations of DAF–2 for 2 h. After irradiation, samples were kept in the dark and measured every 2 h.

2.3.2 Influence of pH, temperature, salinity and wave lengths

The influence of the pH was assessed by adjusting artificial seawater samples to pH levels of 7.1, 7.6 and 8.1 by addition of appropriate amounts of hydrochloric acid (2 mol L^{-1}) or caustic soda solution (2 mol L^{-1}).

To assess the influence of the temperature, artificial seawater samples were adjusted to temperatures of 10 ℃, 20 ℃ and 30 ℃ by controlling the temperature of the thermostat water bath.

To assess the influence of the salinity on the photoproduction of NO from dissolved NO_2^-, artificial seawater samples were adjusted to different salinity of 20, 30 and 35 by adding Milli–Q water or NaCl to the stock solution of artificial seawater.

In order to compare the contributions of ultraviolet A (UVA), ultraviolet B (UVB) and visible light to the NO photoproduction, two kinds of film light filters were used (wrapped around the quartz glass tubes: (i) a Mylar plastic film (from United States Plastic Cor., Lima, Ohio) which can only shield UVB and (ii) a film, always used as car insulation film (from CPFilm Inc., USA) shielding both UVA and UVB.

2.4 Calculations of photoproduction rates (R_{NO}), photoproduction rate constant (J_{NO}) and reaction yield

For the artificial seawater experiments determining the generation of NO from the NO_2^- photochemical degradation, the data were fit with a simple linear regression with the form $y = R_{NO} \times t + b$, where y is the NO concentration which was calculated by the signal intensity of DAF–2T at time t and R_{NO} is the photoproduction rate.

https://doi.org/10.5194/os-2019-57
Preprint. Discussion started: 11 June 2019

The photoproduction rate constant of NO from nitrite (J_{NO}) was determined by preparing different concentrations of NO_2^- (0.5, 2.0 and 5.0 μmol L^{-1}) in Milli–Q water and artificial seawater. The slope of the linear correlation between photoproduction rates and concentrations of NO_2^- represents J_{NO} (Anifowose et al., 2015).

The yield of NO formation ($\%f_{NO}$) from the photodegradation via NO_2^- was estimated according to Anifowose et al. (2015)

$$\%f_{NO} = 100 \times J_{NO} \times c(NO_2^-) \times R_{NO}^{-1}, \quad (2)$$

where $c(NO_2^-)$ is the initial concentration of NO_2^-.

2.5 Seawater samples

Surface seawater samples were collected form a water depth of 1 m during a ship campaign to the western tropical North Pacific Ocean on board the R/V "Dong Fang Hong 2" from 13 November 2015 to 5 January 2016. This cruise covered two sections: a N/S section from 36 to 2 °N along 146/143 °E with 6 and 12 stations, respectively, and a W/E section from 137 to 161 °E along the equator with 13 stations (Fig. 1). Stations S0701 – S0723 were sampled between 11 and 28 November (i.e. the first part of the N/S section), followed by sampling of W/E section between 16 and 27 December and sampling of stations S0725 – S0735 between 30 December 2015 and 05 January 2016 (i.e. second part of the N/S section). In addition, relevant surface currents are indicated in Fig. 1 (Fine et al., 1994; Zhang et al., 2018; Zhao et al., 2016). The location of the Kuroshio Current on 15 November 2015 was taken from https://www1.kaiho.mlit.go.jp/ .

Seawater samples were collected using 8–liter Niskin bottles equipped with silicon O–rings and Teflon–coated springs and mounted on a Sea–Bird CTD (conductivity, temperature, depth) instrument (Sea–Bird Electronics, Inc., USA). Samples were filtered through 0.45 μm and 0.2 μm polyethersulfone membranes (Pall, USA) to minimize microbial influence (Kieber et al., 1996; Yang et al., 2011). Then the filtered seawater was transferred in the dark into acid–cleaned and pre–combusted amber glass bottles, stored in darkness at 4 ℃ (Kieber et al., 1996; Yang et al., 2011) and brought back to the laboratory on land. Samples were re–filtered with 0.2 μm polyethersulfone membranes (Pall, USA) before the irradiation experiments. DAF–2 solutions were added in the dark. The irradiation experiments were conducted within two weeks after the samples arrived in the laboratory.

https://doi.org/10.5194/os-2019-57
Preprint. Discussion started: 11 June 2019

2.6 Dissolved inorganic nitrogen (DIN) and pH measurements

The concentrations of dissolved inorganic nitrogen (DIN = nitrate, nitrite, and ammonium) from the cruise were analyzed using an automated nutrient analyzer (Auto Analyzer 3, SEAL Analytical, USA) onboard. The detection limits were 0.14 μmol L^{-1} for nitrate, nitrite, and ammonium, respectively, with the precision of the method better than +/– 3% (Liu et al., 2005).

The pH values were measured just before the experiments by using a benchtop pH meter (Orion Star A211, Thermo Scientific ™, USA) which was equipped with an Orion 8102 Ross combination pH electrode (Thermo Scientific ™, USA). In order to ensure comparability with the temperature in the irradiation experiments, pH values of the natural seawater samples were measured at 20 ℃. The pH meter was calibrated with three NIST–traceable pH buffers (pH = 4.01, 7.00 and 10.01 at 20 ℃). The precision of pH measurements was +/–0.01.

3 Results and Discussion

3.1 Optimal DAF–2 concentration and storage time

NO concentrations generated from photolysis of artificial seawater samples with an initial NO_2^- concentration of 0.5 μmol L^{-1} increased with increasing DAF–2 concentrations and reached a maximum at a DAF–2 concentration of 1.4 μmol L^{-1} (Fig. 2a). At DAF–2 concentrations >1.4 μmol L^{-1} no further increase of the NO concentrations was observed. Thus, we used a DAF–2 concentration of 1.4 μmol L^{-1} for all experiments.

Samples after reaction with DAF–2 and stored at 4 ℃ in the dark were stable for at least 28 h with the measurement interval about 2 h (Fig. 2b). The relative standard deviations of the resulting NO concentrations after irradiating samples containing 0.5 μmol L^{-1} and 5.0 μmol L^{-1} NO_2^- were +/– 13% and +/– 7%, respectively. This demonstrated that photolysis samples with NO which were allowed to react with DAF–2 could be stored for at least one day at 4 ℃ in the dark.

3.2 Photoproduction of NO in Milli–Q water and artificial seawater

The photoproduction rates of NO in samples with NO_2^- concentrations of 0.5, 2.0 and 5.0 μmol L^{-1} were generally higher in artificial seawater than in Milli–Q water (Fig. 3a and 3b).

https://doi.org/10.5194/os-2019-57
Preprint. Discussion started: 11 June 2019

The resulting J_{NO} were 4.4 ±0.5 ×10^{-4} min^{-1} and 9.4 ±1.4 ×10^{-4} min^{-1} for Milli–Q water and artificial seawater, respectively. They are lower than the J_{NO} of 34.2 ×10^{-4} min^{-1} for Milli–Q water reported by Anifowose et al. (2015). The difference might be explained by different experimental set–ups such the different light sources used in the irradiation experiments.

3.3 Influence of pH, temperature, salinity and wavelengths

All irradiation experiments were conducted in artificial seawater with two different NO_2^- concentrations of 0.5 and 5.0 µmol L^{-1}. The resulting NO concentrations were generally higher when irradiating the samples with the initial NO_2^- concentration of 5.0 µmol L^{-1}. NO photoproduction rates showed increasing trends with decreasing pH, increasing temperatures and increasing salinity (Fig. 4 and 5).

Reaction (1) indicates that decreasing pH which results in lower concentrations of OH^- which, in turn, will promote NO formation via NO_2^-. This is in line with the finding of Li et al (2011) who found that the photodegradation rate of NO_2^- in Milli–Q water was higher at pH = 6.5 than at pH = 9.5.

Higher temperatures led to increasing NO photoproduction rates according to the temperature dependence of chemical reactions given by the Arrhenius formula (k = A exp (−E/RT)) which indicates that an increasing temperature results in a higher rate constant (k).

Higher salinity obviously enhanced photoproduction rates of NO in both Milli–Q water and artificial seawater samples (with 0.5 µmol L^{-1} or 5.0 µmol L^{-1} initial NO_2^- concentrations). This result indicates that with increasing ion strength NO production is enhanced, however, the exact mechanism is unknown. Zafriou and McFarland (1980) demonstrated that artificial seawater comprised with major and minor salts showed complex interactions.

Highest NO photoproduction rates were observed with full wave length band whereas lowest NO rates were observed with UVB. NO photoproduction rates approached zero at wave lengths in the visible. Our results are in line with the findings of Zafiriou and McFarland (1981) who found that samples exposed to (UV+visible) wave lengths lost NO_2^- more rapidly than those exposed only to visible wave lengths alone. Moreover, the photochemical NO_2^- degradation, as described in reaction (1), proceeds at wave lengths of 300–410 nm with a λ_{max} of 356 nm, which is in the range of UVA (320–420 nm) (Zuo and Deng, 1998; Zafiriou and McFarland, 1981).

https://doi.org/10.5194/os-2019-57
Preprint. Discussion started: 11 June 2019

3.4 Kinetics of the NO photoproduction

The yields of NO formation from NO_2^- (%f_{NO}) in Milli–Q water and artificial seawater samples were about 70.1% and 97.9% for the initial NO_2^- concentrations of 0.5 and 5.0 µmol L^{-1}, respectively. The missing NO yield (29.9% for 0.5 µmol L^{-1} and 2.1% for 5.0 µmol L^{-1}) might result from NO production via other (unknown) nitrogen–containing substrates (Anifowose et al., 2015). Assuming a 100% yield from NO_2^- degradation and a fast reaction of NO with DAF–2 the observed linear relationships during the various irradiation experiments (Fig. 6) indicate that NO photoproduction was following a pseudo zero–order reaction. However, the R_{NO} ratios (average: 4.8) listed in Table 2 were not the same for the experiments despite the fact that the ratio of the initial NO_2^- concentrations (= 10) was the same for all experiments. This result, however, does point to reaction which is different from a zero–order reaction.

3.5 Photoproduction rates of NO in the western tropical North Pacific Ocean

During the cruise surface temperatures and salinities were in the range from 22.15 ℃ to 30.19 ℃ and 34.57 to 35.05 respectively. The concentrations of NO_3^-, NH_4^+ and NO_2^- ranged from 0.03 µmol L^{-1} to 1.6 µmol L^{-1}, 0.20 µmol L^{-1} to 1.2 µmol L^{-1} and 0.02 µmol L^{-1} to 0.33 µmol L^{-1}, respectively (Fig. 6). The measured photoproduction rates of NO ranged from 0.3 $\times 10^{-10}$ mol L^{-1} min^{-1} (station S0711) to 2.9 $\times 10^{-10}$ mol L^{-1} min^{-1} (station S0303), with an average value of 13.0 ± 7.6 $\times 10^{-11}$ mol L^{-1} min^{-1}. Photoproduction rates did not show significant correlations with DIN (NO_2^-, NO_3^- or NH_4^+), pH, salinity, water temperature as well as with colored dissolved organic matter (data not shown)(statistics computed with SPSS v.16.0).

The non–existing relationship between R_{NO} and dissolved NO_2^- during our cruise is in contrast to the results of Olasehinde et al. (2010) and Anifowose et al. (2015) who observed positive linear relationships between NO photoproduction rates and the NO_2^- concentrations in the surface waters of the Seto Inland Sea and the Kurose River. However, the NO_2^- concentrations encountered during our cruise (see above) were covering a significantly lower concentration range compared to the NO_2^- concentrations presented in Olasehinde et al. (2010) and Anifowose et al. (2015) which were ranging from 0.4 – 2 µmol L^{-1} and 0 – 60 µmol L^{-1}, respectively.

The average photoproduction rate of NO measured in the cruise is slightly lower than that of Seto Inland Sea and the Bohai/Yellow Seas which could be ascribed to higher background NO_2^- in the river and

https://doi.org/10.5194/os-2019-57
Preprint. Discussion started: 11 June 2019

coastal waters (Olasehinde et al., 2009; Tian et al., 2018) (Table 1). Our result is consistent with the R_{NO} from the central equatorial Pacific Ocean (Zafiriou and McFarland, 1981) (Table 1).

From the T–S diagram (Fig.7), we found that higher photoproduction rates at stations S0701 and S0704 might resulted from the influence of the Kuroshio (see Fig. 1), with enhanced concentrations of NO_2^-. The higher NO production rates measured for stations S0303/S0307 and S0717–S0723 might have been influenced by the South Equatorial and North Equatorial Currents, respectively, but were obviously not associated with enhanced NO_2^- concentrations.

3.6 Flux densities of NO in the surface layer of the WTNP

3.6.1 Air–sea flux density of NO

The NO flux densities were computed with

$$F = k_{sea}([NO] - pNO_{air} \times H^{cp}), \quad (4)$$

for the details of the calculation see (Tian et al., 2018). Since onboard wind speeds were not available, we set the average wind speeds according to (Zhu et al., 2013) to 5 m s^{-1} for the stations S0301 to S0325, to 8.5 m s^{-1} for stations S0701 to S0713, to 7 m s^{-1} for stations S0715 to S0725, and to 6 m s^{-1} for stations S0727 to S0735. We used a value of 10^{-11} (*v*/*v*) for atmospheric NO (Law, 2001). The atmosphere pressure was set to 101.325 kPa. [NO] represents the in–situ NO concentration at the time of sampling during the cruise.

Since measurements [NO] were not available from the cruise we estimated [NO] by assuming that (1) NO production is mainly resulting from NO_2^- photodegradation and (2) the NO photoproduction R_{NO} as measured in our irradiation expereiment is balanced by the NO scavenging rate R_s (Olasehinde et al., 2010; Zafiriou and McFarland, 1981):

$$R_{NO} = [NO] \times R_s, \quad (3)$$

where R_s represents the sum of the rate constants for the scavenging compounds reacting with NO times the concentrations of the scavenger compounds. Taking the reciprocal of the scavenging rate (R_s = 20 s) (Olasehinde et al., 2010), then [NO] was estimated to range from 36 to 330×10^{-12} mol L^{-1}, with an average of 155×10^{-12} mol L^{-1}, which was consistent with previous results (Liu et al., 2017; Olasehinde et al., 2010).

https://doi.org/10.5194/os-2019-57
Preprint. Discussion started: 11 June 2019

The resulting flux density of NO for WTNP ranged from 0.7 to 20 ×10^{-12} mol m^{-2} s^{-1} (with an average of 5.2 ×10^{-12} mol m^{-2} s^{-1}) which is in good agreement with previous estimates (see Table 1).

3.6.2 Oceanic photoproduction rates of NO

The photoproduction rates from our irradiation experiments were extrapolated to the oceanic photoproduction in the WTNP with the equation from (Bange and Uher, 2005; Uher and Andreae, 1996)

$$R_{ocean} = R_{NO} \times \left(\frac{I_{ocean}(1-exp(-K_D \times MLD))}{I_{ss} \times K_D \times MLD}\right), \quad (5)$$

where R_{ocean} and R_{NO} are the photoproduction rates for the ocean mixed layer and seawater irradiation experiments, respectively, see Section 3.5. I_{ocean} and I_{ss} are the average global irradiance at the surface of the ocean mixed layer and the solar simulator used here, K_D is the light attenuation coefficient and MLD is the estimated mixed layer depth at the sampled station.

I_{ocean} was set to 185 W m^{-2}, while I_{ss} was 725 W m^{-2} in our study (Bange and Uher, 2005; Wu et al., 2015). As described above, UVA is the most influencing wavelength and it is reported that 365 nm is primarily responsible for NO production (Liang and Cort, 2007; Li et al., 2011; Zafiriou and McFarland, 1981). K_{D-365} ranges from 0.03 in clean water to 0.3 in turbid water (Lee et al., 2013). We use 0.1 as the average K_D value in our study. The MLD was taken as the layer depth where the temperature was 0.2 ℃ lower than the 10 m near–face seawater layer (Montégut, 2004), ranging from 13 – 77 m. The resulting average R_{ocean} was about 8.6 ±4.9 ×10^{-12} mol L^{-1} min^{-1} for the WTNP at the time of our cruise. Besides, the temperature at 20 ℃ in our laboratory experiment would induce about 10% error (Fig. 4e).

NO photoproduction seems to be larger than the NO sea–air flux density which indicates that other loss pathways for NO existed in the surface waters of the WTNP.

Conclusion

The results of our irradiation experiments showed that NO photoproduction from NO_2^- in artificial seawater is significantly affected by changes in pH, temperature and salinity. We found increasing NO production rates from dissolved NO_2^- with decreasing pH, increasing temperatures and increasing salinity. In contrast we did not find any correlations of NO photoproduction with pH, salinity, water temperature as well as dissolved NO_2^- in natural surface seawater samples from a cruise to the western tropical North Pacific Ocean (November 2015 – January 2016). We conclude that the trends observed in

https://doi.org/10.5194/os-2019-57
Preprint. Discussion started: 11 June 2019

our irradiation experiments with artificial seawater do not seem to be representative for WTNP because of the complex settings of open ocean environments. Moreover, we conclude that future changes of NO photoproduction due to ongoing environmental changes such as ocean warming and acidification are, therefore, difficult to predict and need to be tested by irradiation experiments of natural seawater samples under varying conditions. A comparison of the oceanic NO photoproduction rates from the WTNP with estimates of the NO air–sea flux densities showed that the photoprodcution rates were significantly larger than the air–sea flux densities. This indicates a further NO loss process in the surface layer of the WTNP. In order to decipher and to quantify the NO production and consumption pathways in the oceanic surface layer more comprehensive laboratory and onboard measurements are required.

Author contributions.

YT, GY, CL, HC and PL prepared the original manuscript and designed the experiments; HB made many modifications and gave a lot of suggestions on design of figures and the computing method. All authors contributed to the analysis of the data and discussed the results.

Competing interests.

The authors declare that they have no conflict of interest.

Acknowledgement

We thank the captain and crew of the R/V “Dong Fang Hong 2” for their support and help during the cruise. This research was supported by the National Natural Science Foundation of China (Nos.41676065), the National Key Research and Development Program of China (Grant No. 2016YFA0601301), and the Fundamental Research Funds for the Central Universities (No. 201762032).

References

Anifowose, A. J., Takeda, K., and Sakugawa, H.: Photoformation rate, steady–state concentration and lifetime of nitric oxide radical (NO ·) in a eutrophic river in Higashi–Hiroshima, Japan, Chemosphere, 119, 302–309,2015.

Astier, J., Jeandroz, S., and Wendehenne, D.: Nitric oxide synthase in plants: The surprise from algae, Plant Sci., 268, 64–66, 2018.

Bajt, O., Šket, B., and Faganeli, J.: The aqueous photochemical transformation of acrylic acid, Mar. Chem., 58, 255–259, 1997.

https://doi.org/10.5194/os-2019-57
Preprint. Discussion started: 11 June 2019

Bange, H. W., and Uher, G.: Photochemical production of methane in natural waters: implications for its present and past oceanic source, Chemosphere, 58, 177–183, 2005.

Bange, H. W.: Gaseous Nitrogen Compounds (NO, N_2O, N_2, NH_3) in the Ocean, Elsevier 51–94 pp., 2008.

Fine, R. A., Lukas, R., Bingham, F. M., Warner, M. J., and Gammon, R. H.: The western equatorial Pacific: A water mass crossroads, J. Geophys. Res.: Oceans, 99, 25063–25080, 1994.

Kieber, D. J., Jiao, J., Kiene, R. P., and Bates, T. S.: Impact of dimethylsulfide photochemistry on methyl sulfur cycling in the Equatorial Pacific Ocean, J. Geophys. Res.: Oceans, 101, 3715–3722, 1996.

Kuypers, M. M. M., Marchant, H. K., and Kartal, B.: The microbial nitrogen–cycling network, Nat. Rev. Microbiol.,16, 263–276, 2018.

Law, C. S.: Air–sea transfer: N_2O, NO, CH_4 , CO, Encyclopedia of Ocean Sciences, 137–144, 2001.

Lee, Z., Hu, C., Shang, S., Du, K., Lewis, M., Arnone, R., and Brewin, R.: Penetration of UV–visible solar radiation in the global oceans: Insights from ocean color remote sensing: penetration of uv–visible solar light, J. Geophys. Res.: Oceans, 118, 4241–4255, 2013.

Li, P. F., Li, W. S., Liu, C. Y., Zhu, X. C., and Zhang, Q.: The photodecomposition of nitrite in water, Environ. Chem., 30, 1883–1888, 2011.

Liang, C., and Cort, A.: Temperature and wavelength dependence of nitrite photolysis in frozen and aqueous solutions, Environ. Sci. Technol., 41, 3626–3632, 2007.

Liu, C.–Y., Feng, W.–H., Tian, Y., Yang, G.–P., Li, P.–F., and Bange, H. W.: Determination of dissolved nitric oxide in coastal waters of the Yellow Sea off Qingdao, Ocean Sci., 13, 623–632, 2017.

Liu, S. M., Zhang, J., Chen, H. T., and Zhang, G. S.: Factors influencing nutrient dynamics in the eutrophic Jiaozhou Bay, North China, Prog Oceanogr, 66, 66–85, 2005.

Lutterbeck, H. E., and Bange, H. W.: An improved method for the determination of dissolved nitric oxide (NO) in seawater samples, Ocean Sci., 11, 959–981, 2015.

Montégut, C. D. B.: Mixed layer depth over the global ocean: An examination of profile data and a profile–based climatology, J. Geophys. Res.: Oceans, 109, c12003, 2004.

Olasehinde, E. F., Takeda, K., and Sakugawa, H.: Development of an analytical method for nitric oxide radical determination in natural waters, Anal. Chem., 81, 6843–6850, 2009.

Olasehinde, E. F., Takeda, K., and Sakugawa, H.: Photochemical production and consumption mechanisms of nitric oxide in seawater, Environ. Sci. Technol., 44, 8403–8408, 2010.

Schreiber, F., Wunderlin, P., Udert, K. M., and Wells, G. F.: Nitric oxide and nitrous oxide turnover in natural and engineered microbial communities: biological pathways, chemical reactions, and novel technologies, Front Microbiol., 3, 372, 2012.

Singh, V. K., and Lal, B.: Nitric oxide (NO) stimulates steroidogenesis and folliculogenesis in fish, Reproduction, 153, 133, 2016.

Tian, Y., Xue, C., Liu, C. Y., Yang, G. P., Li, P. F., Feng, W. H., and Bange, H. W.: Nitric oxide (NO) in the Bohai and Yellow Seas, Biogeosciences Discuss., 1–25, 2018.

Uher, G., and Andreae, M. O.: The diel cycle of carbonyl sulfide in marine surface waters: Field study results and a simple model, Aquat. Geochem., 2, 313–344, 1996.

Wang, B., Dan, L., Chao, W., Wang, Q., Hui, Z., Liu, G., Xia, T., and Zhang, L.: Mechanism of endothelial nitric oxide synthase phosphorylation and activation by tentacle extract from the jellyfish Cyanea capillata, Peerj, 5, e3172, 2017.

Wu, X., Liu, C. Y., and Li, P. F.: Photochemical transformation of acrylic acid in seawater, Mar. Chem., 170, 29–36, 2015.

https://doi.org/10.5194/os-2019-57
Preprint. Discussion started: 11 June 2019

Yang, G. P., Ren, C. Y., Lu, X. L., Liu, C. Y., and Ding, H. B.: Distribution, flux, and photoproduction of carbon monoxide in the East China Sea and Yellow Sea in spring, J. Geophys. Res.: Oceans, 116, –, 2011.

Zafiriou, O. C., and True, M. B.: Nitrite photolysis in seawater by sunlight ☆, Mar. Chem., 8, 33–42, 1979.

Zafiriou, O. C., Mcfarland, M., and Bromund, R. H.: Nitric oxide in seawater, Science, 207, 637, 1980.

Zafiriou, O. C., and McFarland, M.: Nitric oxide from nitrite photolysis in the central equatorial Pacific, J. Geophys. Res.: Oceans, 86, 3173–3182, 1981.

Zhang, Z., Qiu, B., Tian, J., Zhao, W., and Huang, X.: Latitude–dependent finescale turbulent shear generations in the Pacific tropical–extratropical upper ocean, Nat. Commun., 9, 4086, 2018.

Zhao, J., Li, Y., and Wang, F.: Seasonal variation of the surface North Equatorial Countercurrent (NECC) in the western Pacific Ocean, Chin. J. Oceanol. Limnol., 34, 1332–1346, 2016.

Zhu, M., Jia, B., Zheng, C., and Liu, Z.: Characteristics of sea surface wind speed in the northwest Pacific, Meteorological Hydrological and Marine Instruments,30,125–128, 2013.(in Chinese with English abstract)

Zuo, Y., and Deng, Y.: The near–UV absorption constants for nitrite ion in aqueous solution, Chemosphere, 36, 181–188, 1998.

https://doi.org/10.5194/os-2019-57
Preprint. Discussion started: 11 June 2019

Figure Captions

Fig. 1. Locations of the sampling stations in the western tropical North Pacific Ocean. The acronyms NGCC, SEC, NECC, NEC, and STCC stand for New Guinea Coastal Current, South Equatorial Current, North Equatorial Counter Current, North Equatorial Current, and Subtropical Counter Current, respectively.

Fig. 2. Changes of NO concentrations with initial DAF–2 concentration of 0, 0.7, 1.4, 2.1, 2.8, 3.5 and 4.2 μmol L^{-1} after irradiation time of 2 h (a) and changes of different NO concentrations with storage time monitored at about 2 h time intervals (b).

Fig. 3. Photoproduction rates of NO with 0.5, 2, and 5.0 μmol L^{-1} NO_2^- (a) and the calculated J_{NO} values in Milli–Q water and artificial seawater (b), symbols in red represented for the artificial seawater samples and in black for Milli–Q water.

Fig. 4. NO concentration changes with irradiation time at different pH, salinity, temperature and waveband conditions (a, c, e, g for 0.5 μmol L^{-1} NO_2^- and b, d, f, h for 5.0 μmol L^{-1} NO_2^-).

Fig. 5. Changes of NO photoproduction rates with irradiation time at different pH, salinity, temperature and waveband conditions (a, c, e, g for 0.5 μmol L^{-1} NO_2^- and b, d, f, h for 5.0 μmol L^{-1} NO_2^-).

Fig. 6. Seawater temperature, salinity, concentrations of NO_2^-, NO_3^-, NH_4^+, and photoproduction rates of NO (R_{NO}) in the western tropical North Pacific Ocean. (a: W/E transect; b: N/S transect)

Fig. 7. The potential temperature–salinity (T–S) diagram with NO photoproduction rates indicated in the color bar. Water mass characteristics of surface currents shown in Figure 1 are indicated. The acronyms NGCC, SEC, NECC, NEC, and STCC stand for New Guinea Coastal Current, South Equatorial Current, North Equatorial Counter Current, North Equatorial Current, and Subtropical Counter Current, respectively.

https://doi.org/10.5194/os-2019-57
Preprint. Discussion started: 11 June 2019

Ocean Science
Discussions
Open Access
EGU

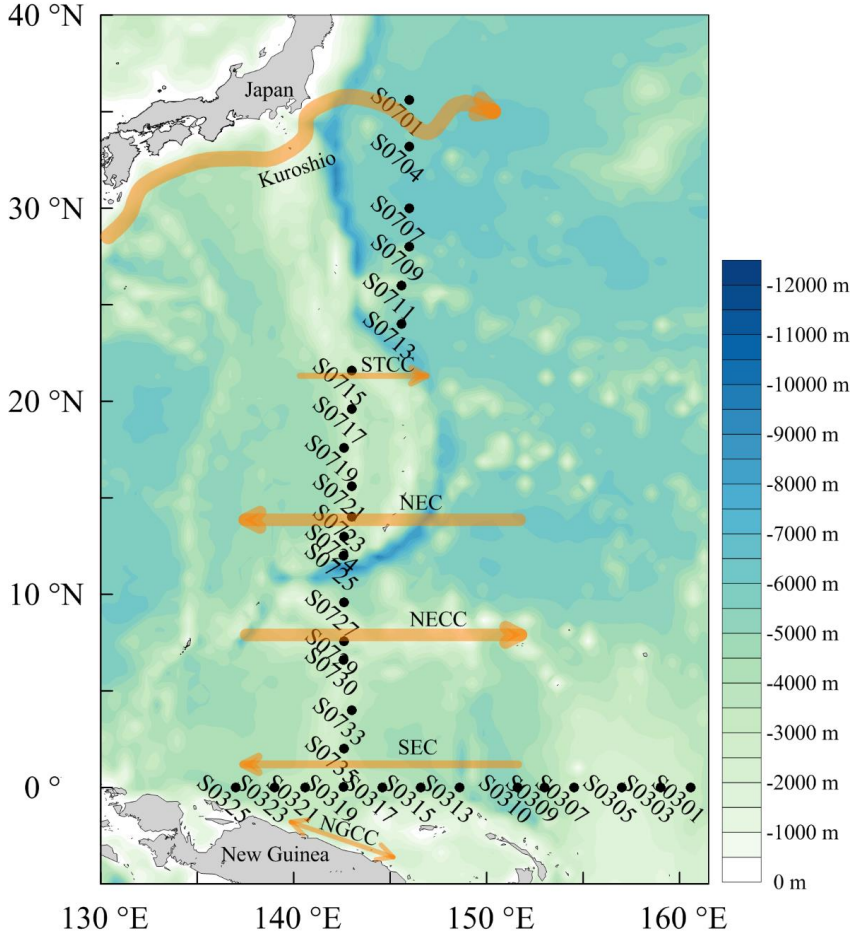

Fig. 1. Locations of the sampling stations in the western tropical North Pacific Ocean. The acronyms NGCC, SEC, NECC, NEC, and STCC stand for New Guinea Coastal Current, South Equatorial Current, North Equatorial Counter Current, North Equatorial Current, and Subtropical Counter Current, respectively.

https://doi.org/10.5194/os-2019-57
Preprint. Discussion started: 11 June 2019

Ocean Science
Discussions
Open Access
EGU

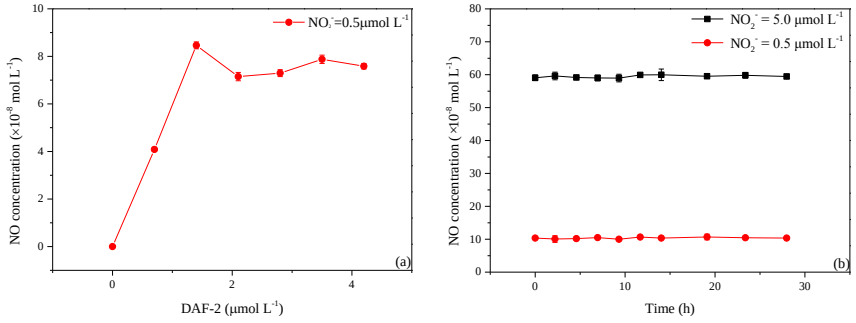

Fig. 2. Changes of NO concentrations with initial DAF–2 concentration of 0, 0.7, 1.4, 2.1, 2.8, 3.5 and 4.2 μmol L^{-1} after irradiation time of 2 h (a) and changes of different NO concentrations with storage time monitored at about 2 h time intervals (b).

https://doi.org/10.5194/os-2019-57
Preprint. Discussion started: 11 June 2019

Ocean Science
Discussions
Open Access
EGU

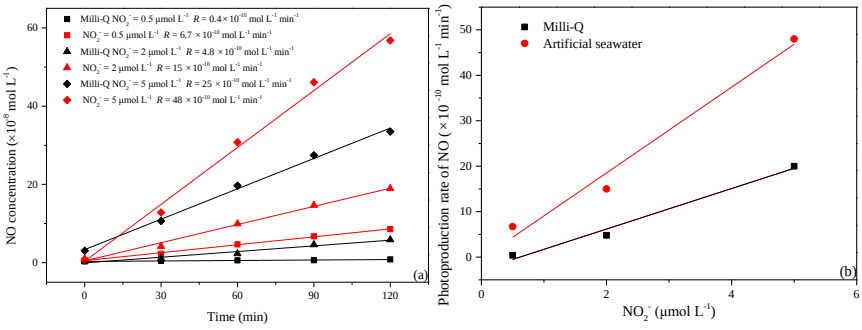

400 **Fig. 3.** Photoproduction rates of NO with 0.5, 2, and 5.0 μmol L^{-1} NO_2^- (a) and the calculated J_{NO} values in Milli–Q water and artificial seawater (b), symbols in red represented for the artificial seawater samples and in black for Milli–Q water.

https://doi.org/10.5194/os-2019-57
Preprint. Discussion started: 11 June 2019

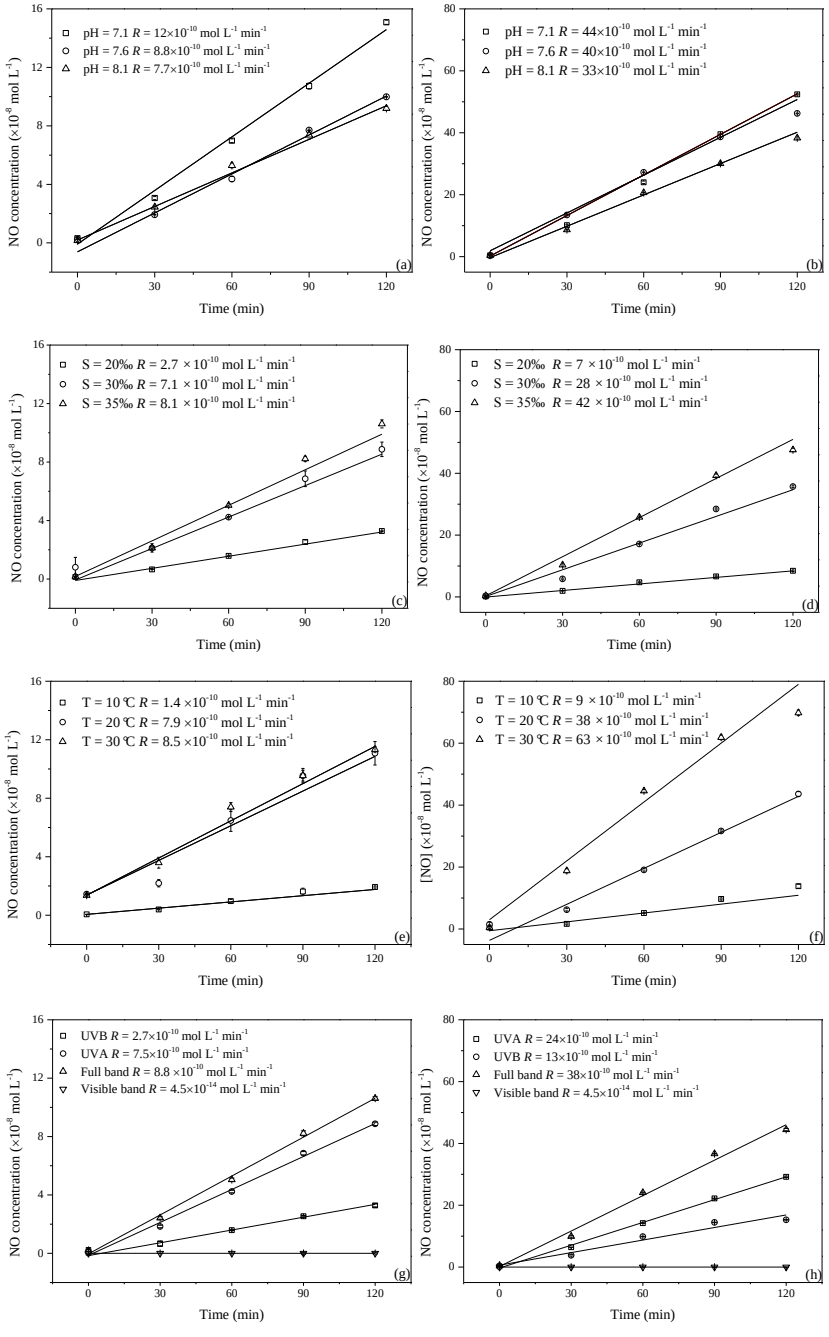

405

Fig. 4. NO concentration changes with irradiation time at different pH, salinity, temperature and waveband conditions (a, c, e, g for 0.5 μmol L^{-1} NO_2^- and b, d, f, h for 5.0 μmol L^{-1} NO_2^-).

410

https://doi.org/10.5194/os-2019-57
Preprint. Discussion started: 11 June 2019

Ocean Science
Discussions
Open Access
EGU

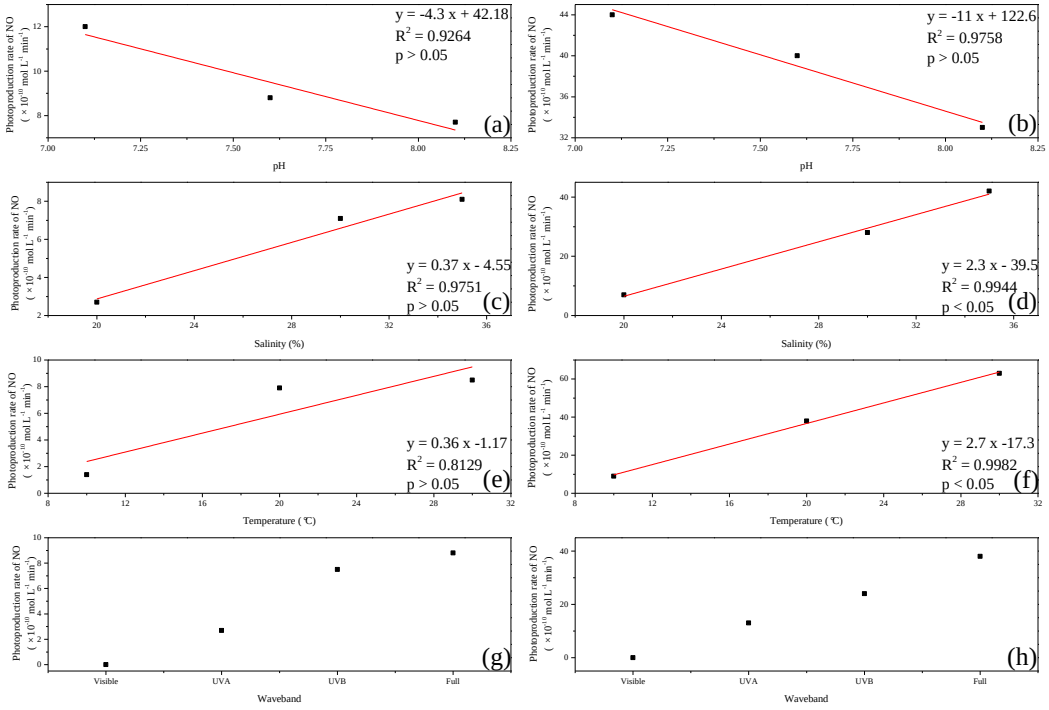

Fig. 5. Changes of NO photoproduction rates with irradiation time at different pH, salinity, temperature and waveband conditions (a, c, e, g for 0.5 μmol L^{-1} NO_2^- and b, d, f, h for 5.0 μmol L^{-1} NO_2^-).

https://doi.org/10.5194/os-2019-57
Preprint. Discussion started: 11 June 2019

Ocean Science
Discussions
Open Access
EGU

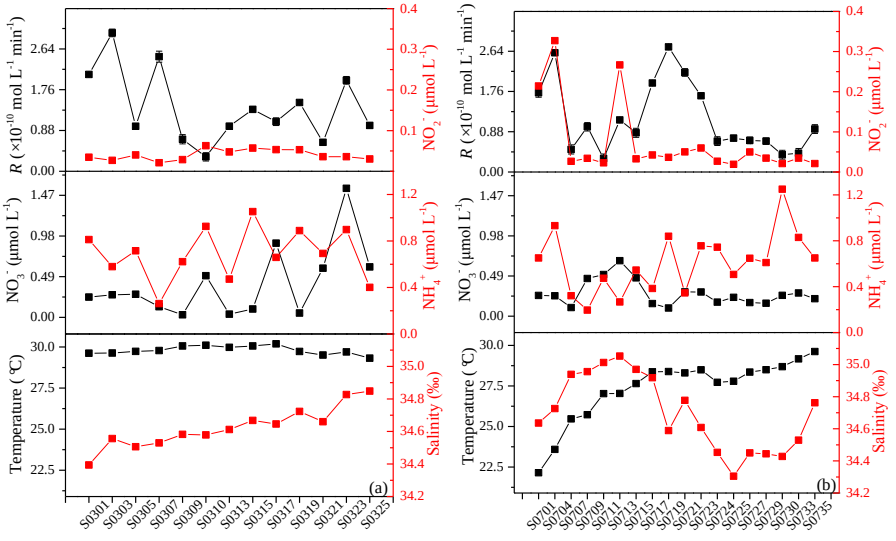

Fig. 6. Seawater temperature, salinity, concentrations of NO_2^-, NO_3^-, NH_4^+, and photoproduction rates of NO (R_{NO}) in the western tropical North Pacific Ocean (a: W/E transect; b: N/S transect.).

420

https://doi.org/10.5194/os-2019-57
Preprint. Discussion started: 11 June 2019

Ocean Science
Discussions
Open Access
EGU

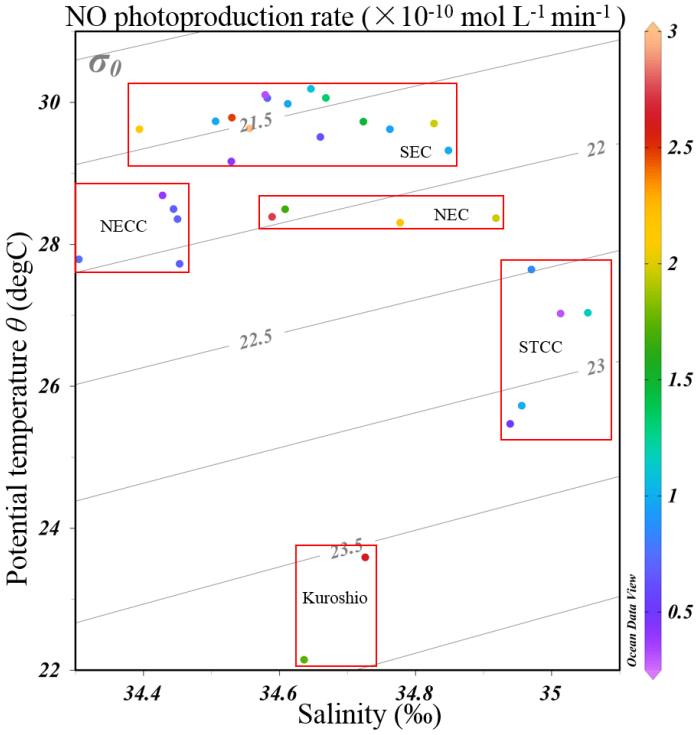

Fig. 7. The potential temperature–salinity (T–S) diagram with NO photoproduction rates indicated in the color bar. Water mass characteristics of the surface currents shown in Figure 1 are indicated. The acronyms NGCC, SEC, NECC, NEC, and STCC stand for New Guinea Coastal Current, South Equatorial Current, North Equatorial Counter Current, North Equatorial Current, and Subtropical Counter Current, respectively.

https://doi.org/10.5194/os-2019-57
Preprint. Discussion started: 11 June 2019

Ocean Science
Discussions
Open Access
EGU

Table Captions

Table 1 Photoproduction rates (*R*), average NO concentrations and average flux densities of NO in different regions.

Table 2 The ratios of photoproduction rates (*R*5.0/*R*0.5) in the different irradiation experiments.

https://doi.org/10.5194/os-2019-57
Preprint. Discussion started: 11 June 2019

Table 1 Photoproduction rates (*R*),average NO concentrations and average flux densities of NO in different regions.

Regions	*R* (mol L^{-1} s^{-1})	NO (mol L^{-1})	Flux (mol m^{-2} s^{-1})	Sampling date	References
Seto Inland Sea, Japan	$8.7–38.8\times10^{-12}$	120×10^{-12}	3.55×10^{-12}	October 5–9, 2009	Olasehinde et al., 2010
Jiaozhou Bay	–	157×10^{-12}	7.2×10^{-12}	June, July and August, 2010	Tian et al., 2016
Jiaozhou Bay and its adjacent waters	–	$(160\pm130)\times10^{-12}$	10.9×10^{-12}	March 8–9, 2011	Xue et al., 2011
Kurose River, Japan	$9.4–300\times10^{-12}$	–	–	–	Olasehinde et al., 2009
Kurose River, Japan	$1–3950\times10^{-12}$	$0.02–68.5\times10^{-12}$	–	January and December 2013	Anifowose et al., 2015
Central equatorial Pacific	$> 10^{-12}$	46×10^{-12}	2.2×10^{-12}	R/V Knorr 73/7	Zafiriou and Mcfarland., 1981
Bohai Sea and Yellow Sea	$10.1\pm12.3\times10^{-12}$	174×10^{-12}	4.5×10^{-12}	June 13–28, 2011	Personal disscussion
The northwest Pacific Ocean	$2.1\pm1.3\times10^{-12}$	153×10^{-12}	5.2×10^{-12}	November 15, 2015 to January 26, 2016	This study

https://doi.org/10.5194/os-2019-57
Preprint. Discussion started: 11 June 2019

Ocean Science
Discussions
Open Access
EGU

Table 2 The ratios of photoproduction rates (*R*5.0/*R*0.5) in the different irradiation experiments.

	R ($\times 10^{-10}$ mol L^{-1} min^{-1})		Ratio
	0.5 μM	5.0 μM	
pH=7.1	12	44	3.7
pH=7.6	8.8	40	4.5
pH=8.1	7.7	33	4.3
T=10 ℃	1.4	9.0	6.4
T=20 ℃	7.9	38	4.8
T=30 ℃	8.5	63	7.4
S=20	2.7	7.0	2.6
S=30	7.1	28	3.9
S=35	8.1	42	5.2